particles

IMPACT FACTOR 1.7

CITESCORE 3.2

Article

Galactic Stellar Black Hole Binaries: Spin Effects on Jet Emissions of High-Energy Gamma-Rays

Dimitrios Rarras, Theocharis Kosmas, Theodora Papavasileiou and Odysseas Kosmas

MDPI

https://doi.org/10.3390/particles7030046

particles

MDPI

Article

Galactic Stellar Black Hole Binaries: Spin Effects on Jet Emissions of High-Energy Gamma-Rays

Dimitrios Rarras [1,†], Theocharis Kosmas [1,*,†], Theodora Papavasileiou [1,2,†] and Odysseas Kosmas [1,†,‡]

[1] Department of Physics, University of Ioannina, GR-45110 Ioannina, Greece; rarrasdimitrios@gmail.com (D.R.); th.papavasileiou@uowm.gr (T.P.); odykosm@gmail.com (O.K.)
[2] Department of Informatics, University of Western Macedonia, GR-52100 Kastoria, Greece
* Correspondence: hkosmas@uoi.gr; Tel.: +30-2651-008-489
† These authors contributed equally to this work.
‡ Current address: Conigital Ltd., 51 Parkside, Coventry CV1 2HG, UK.

Abstract: In the last few decades, galactic stellar black hole X-ray binary systems (BHXRBs) have aroused intense observational and theoretical research efforts specifically focusing on their multi-messenger emissions (radio waves, X-rays, γ-rays, neutrinos, etc.). In this work, we investigate jet emissions of high-energy neutrinos and gamma-rays created through several hadronic and leptonic processes taking place within the jets. We pay special attention to the effect of the black hole's spin (Kerr black holes) on the differential fluxes of photons originating from synchrotron emission and inverse Compton scattering and specifically on their absorption due to the accretion disk's black-body radiation. The black hole's spin (dimensionless spin parameter a_*) enters into the calculations through the radius of the innermost circular orbit around the black hole, the R_{ISCO} parameter, assumed to be the inner radius of the accretion disk, which determines its optical depth τ_{disk}. In our results, the differential photon fluxes after the absorption effect are depicted as a function of the photon energy in the range 1 GeV$\leq E \leq 10^3$ GeV. It is worth noting that when the black holes' spin (α_*) increases, the differential photon flux becomes significantly lower.

Keywords: stellar black holes; galactic XRBs; Kerr black holes; black hole spin; photon jet emissions; photon flux

Citation: Rarras, D.; Kosmas, T.; Papavasileiou, T.; Kosmas, O. Galactic Stellar Black Hole Binaries: Spin Effects on Jet Emissions of High-Energy Gamma-Rays. *Particles* **2024**, *7*, 792–804. https://doi.org/10.3390/particles7030046

Academic Editor: Robert Vertesi

Received: 10 July 2024
Revised: 26 August 2024
Accepted: 30 August 2024
Published: 3 September 2024

1. Introduction

In the last few decades, one of the powerful techniques to test the Kerr nature of astrophysical black holes, based on the study of the electromagnetic reflection spectrum of accretion disks, is considered X-ray reflection spectroscopy (see, for example, Refs. [1–9]). As it is well known, the accretion disk of black holes emits thermal photons that can exhibit inverse Compton scattering off free electrons in the compact object's corona, which is a hot and optically thin medium close to the stellar black hole object.

Stellar-mass black holes are formed either from the gravitational collapse of massive stars or from the merger of two neutron stars. For our purposes, stellar-mass black holes have masses ranging from $M_{BH} \approx 3M_{\odot}$ up to $M_{BH} \approx 50M_{\odot}$, specifically similar to the mass of the donor star of the BHXRB system.

In this work, we deal with uncharged ($Q = 0$) black holes which are classified in two categories, i.e., Schwarzschild black holes (non-rotating, $J = 0$) that were the first exact solution of Einstein's field equations found by Karl Schwarzschild in 1916, and Kerr black holes (rotating, $J \neq 0$) that were found by Roy Kerr (1963) (see Ref. [10]). We mention that charged ($Q \neq 0$) black holes are either Reissner–Nordström (non-rotating, $J = 0$) or Kerr–Newman (rotating, $J \neq 0$) types (see Ref. [11] pp. 33–58). The Kerr–Newman metric of a charged spinning black hole is the most general BH solution, which was found by Ezra "Ted" Newman in 1965 (see Ref. [12]). It is worth mentioning that all astrophysical black

holes (BHs) can be described by the Kerr metric with only two parameters: (i) the black hole mass (M_{bh}) and (ii) the black hole angular momentum (J).

In the present work, we study jet emissions of radiation and neutrinos created through several hadronic and leptonic processes occurring inside the jets. We focus on the effect of the black hole's spin (Kerr black holes) on the differential photon fluxes and specifically on the absorption effect which is mainly due to the accretion disk's black-body radiation. We mention that the black hole's spin (dimensionless spin parameter a_*) enters this type of calculation through the radius of the innermost circular orbit around the black hole, i.e., the R_{ISCO} geometrical parameter, assumed to be the inner radius of the accretion disc. This parameter determines the optical depth, τ_{disk}, of the accretion disc.

Recently, progress has been made in measuring the spins of stellar-mass BHs in the Milky Way Galaxy (see Ref. [13] and references therein). Independent determinations of the BHs' spins are of fundamental importance for testing general relativity (GR) and for a deep understanding of space and time.

The rest of this paper is organized as follows. In Section 2, we make a brief description of the state of the art of Kerr black holes with the assumed metric. In Section 3, analytic calculations of the emitted photon differential flux carried out within the above model are presented and discussed. In addition, the absorption effects due to photon annihilation and e^+, e^- pair creation are considered. Finally, in Section 4, the extracted conclusions from the aforementioned investigation are summarized and future work that is planned is briefly shortly discussed.

2. Background—Description of the Model

In this section, we discuss the radius of the innermost stable circular orbit in the Kerr geometry—the Kerr R_{ISCO}—the main interactions that take place inside the jets, the transfer equation which describes the particles' energy distribution inside the jets, the source function of gamma-rays, the intensity and integral flux of gamma-rays, and the absorption of photons.

2.1. Kerr R_{ISCO}

In previous works (see Refs. [14–16]), the black hole of the binary system was supposed to be a Schwarzschild black hole, with its only property being that of the mass. However, this case is not realistic, as most of the black holes, besides possessing mass M, also have angular momentum J. For this reason, in this work, we consider the black hole to be a Kerr black hole, one that has mass and is rotating.

The line element of the Kerr geometry (see Ref. [11] pp. 49–52 and also Ref. [17]), describing the space–time around a Kerr black hole, is

$$\begin{aligned} ds^2 = c^2\left(1 - \tfrac{2\mu r}{\rho^2}\right)dt^2 + \tfrac{4\mu\alpha c r \sin^2\theta}{\rho^2}dtd\phi - \tfrac{\rho^2}{\Delta}dr^2 \\ -\rho^2 d\theta^2 - \left(r^2 + \alpha^2 + \tfrac{2\mu r\alpha^2 \sin^2\theta}{\rho}\right)\sin^2\theta d\phi^2 \end{aligned} \quad (1)$$

where $\mu = r_g = \frac{r_S}{2} = \frac{GM}{c^2}$ and $\alpha = \frac{J}{Mc}$ are constants. Furthermore,

$$\rho^2 = r^2 + \alpha^2\cos^2\theta, \qquad \Delta = r^2 - 2\mu r + \alpha^2.$$

The above expression for ds^2 is known as the *Boyer–Lindquist form* and that for (t, r, θ, ϕ) as *Boyer–Lindquist coordinates*. It is useful to define the dimensionless *spin parameter* $\alpha_* \equiv \alpha/\mu$. The larger this parameter, the more aspherical the line element. The case of $\alpha_* = 1$ corresponds to an *extreme* Kerr black hole. Schwarzschild black holes are the special case for $\alpha_* = 0$.

We are now going to derive the innermost stable circular orbit, R_{ISCO}, around a Kerr black hole. To do so, we work on the equatorial plane; setting $\theta = \pi/2$ in the Kerr line element of Equation (1), we obtain

$$ds^2 = c^2\left(1 - \frac{2\mu}{r}\right)dt^2 + \frac{3\mu\alpha c}{r}dtd\phi - \frac{r^2}{\Delta}dr^2 - \left(r^2 + \alpha^2 + \frac{2\mu\alpha^2}{r}\right)d\phi^2 \tag{2}$$

from which we can read the covariant metric components $g_{\mu\nu}$ and calculate the contravariant metric components $g^{\mu\nu}$. We take a particle with unit rest mass such that $p^\mu = \frac{dx^\mu}{d\tau}$. Since the metric does not depend explicitly on t and ϕ, we obtain p_t and p_ϕ that are conserved:

$$p_t = kc^2, \quad p_\phi = -h \tag{3}$$

where k and h are constants that represent the energy and the angular momentum of the particle. We use the fact that $g^{\mu\nu}p_\mu p_\nu = c^2$. Since $p_\theta = 0$ and substituting Equation (3), after some elaboration, we obtain the energy equation:

$$\frac{1}{2}\left(\frac{dr}{d\tau}\right)^2 + V_{eff}(r;h,k) = \frac{1}{2}c^2(k^2-1) \tag{4}$$

where we have identified the effective potential per unit mass as

$$V_{eff}(r;h,k) = -\frac{\mu c^2}{r} + \frac{h^2 - \alpha^2c^2(k^2-1)}{2r^2} - \frac{\mu(h-\alpha ck)^2}{r^3} \tag{5}$$

Circular motion occurs when $\left(\frac{dr}{d\tau}\right)^2 = 0$, and to remain in a circular motion, the radial acceleration $\frac{d^2r}{d\tau^2}$ must also vanish. In terms of the effective potential, we require

$$V_{eff}(r;h,k) = \frac{1}{2}c^2(k^2-1) \quad and \quad \frac{dV_{eff}}{dr} = 0 \tag{6}$$

For a circular orbit to also be stable, we require that

$$\frac{d^2V_{eff}}{dr^2} = 0 \tag{7}$$

From this, we obtain an implicit equation for the coordinate radius of the innermost stable circular orbit, see Ref. [11] pp. 49–52 and also Ref. [17]:

$$r^2 - 6\mu r - 3\alpha^2 \pm 8\alpha\sqrt{\mu r} = 0 \tag{8}$$

where the upper sign corresponds to an orbit of a co-rotating particle, with respect to the black hole's spin, and the lower sign to an orbit of a counter-rotating particle. The solution to Equation (8) (see Ref. [18]), the R_{ISCO}, is found to be

$$R_{ISCO} = \mu\{3 + Z_2 \mp [(3-Z_1)(3+Z_1+2Z_2)]^{1/2}\} \tag{9}$$

where

$$Z_1 \equiv 1 + \left(1-\alpha_*^2\right)^{1/3}\left[(1+\alpha_*)^{1/3} + (1-\alpha_*)^{1/3}\right]$$
$$Z_2 \equiv \left(3\alpha_*^2 + Z_1^2\right)^{1/2}$$

In the limit $\alpha_* = 0$, we recover $R_{ISCO} = 6r_g$, the Schwarzschild case. In the extreme Kerr limit $\alpha_* = 1$, we find $R_{ISCO} = 9r_g$ for the counter-rotating orbit and $R_{ISCO} = r_g$ for the co-rotating case. We conclude that R_{ISCO} strongly depends on the spin (angular momentum) of the black hole and, respectively, whether the particle is counter- or co-rotating. This radius plays a crucial role when we calculate the absorption from the accretion disc as, in our model, it is the inner radius of the accretion disk, R_{in}.

2.2. Main Reactions Inside the Jets

For the production of gamma-rays and neutrinos, two chains of reactions take place inside the jet. Specifically, the relativistic protons of the jet interact mainly with the cold hadronic matter of the jet, as well as with photons created from internal and external emission sources (see Refs. [19–21]).

The first chain of reactions begins with the proton–proton, $p-p$, collisions which are

$$\begin{aligned} pp &\longrightarrow pp + \alpha\pi^0 + \beta\pi^+\pi^- \\ pp &\longrightarrow pn + \pi^+ + \alpha\pi^0 + \beta\pi^+\pi^- \\ pp &\longrightarrow nn + 2\pi^+ + \alpha\pi^0 + \beta\pi^+\pi^- \end{aligned} \tag{10}$$

where α and β are multiplicities depending on the proton energy (see Ref. [22]).

The second chain of reactions begins with proton–photon, $p-\gamma$ scatterings, which are

$$\begin{aligned} p\gamma &\longrightarrow n\pi^+ \\ p\gamma &\longrightarrow p\pi^0 \\ p\gamma &\longrightarrow p\pi^0\pi^+\pi^- \end{aligned} \tag{11}$$

Subsequently, the pion decay processes take place as follows. The neutral pion decays to two gamma-ray photons:

$$\pi^0 \longrightarrow \gamma + \gamma \tag{12}$$

While the charged pions decay to muons and muon-neutrinos, the muons (antimuons) decay to electrons (positrons) and electron-neutrinos (electron-antineutrinos):

$$\begin{aligned} \pi^+ &\longrightarrow \mu^+\nu_\mu \longrightarrow e^+\bar{\nu}_\mu\nu_e + \nu_\mu \\ \pi^- &\longrightarrow \mu^-\bar{\nu}_\mu \longrightarrow e^-\nu_\mu\bar{\nu}_e + \bar{\nu}_\mu \end{aligned} \tag{13}$$

2.3. The Transfer Equation

The governing equation that describes the matter inside the jet, in its simplest form, is the steady-state transfer equation (see Refs. [23–25]):

$$\frac{\partial N(E,z)b(E,z)}{\partial E} + t^{-1}N(E,z) = Q(E,z) \tag{14}$$

where its solution $N(E,z)$ is the energy distributionof the particles inside the jet. $Q(E,z)$ is the particle source function giving the respective production rate. $b(E)$ is the energy loss rate, which has the form $b(E) = dE/dt = -E \cdot t_{loss}^{-1}$, with t_{loss}^{-1} being the rate that the particles lose energy. The rate t^{-1} is given as the sum $t^{-1} = t_{esc}^{-1} + t_{dec}^{-1}$, with $t_{esc}^{-1} = c/(z_{max} - z_0)$ being the rate that the particles escape the acceleration zone and t_{dec}^{-1} their decay rate.

The solution of the transfer equation is (see Refs. [26–28]):

$$N(E,z) = \frac{1}{|b(E)|}\int_E^{E_{max}} Q(E',z)e^{-\tau(E,E')}dE' \tag{15}$$

where

$$\tau(E,E') = \int_E^{E'} \frac{t^{-1}}{|b(E'')|}dE'' \tag{16}$$

The transfer equation is to be solved numerically. For each particle in the chains of reactions, we have a different transfer equation. The particles that are produced from others have a dependence on them through their source function. So, the set of transfer equations becomes a set of coupled equations.

In recent research, a more general form of the transfer equation is being used [29,30], that is,

$$\frac{\partial N(E,t,z)}{\partial t}+\frac{\partial(\Gamma(t,z)v(t,z)N(E,t,z))}{\partial z}+\frac{\partial N(E,t,z)b(E,t,z)}{\partial E}+t^{-1}N(E,t,z)=Q(E,t,z) \quad (17)$$

The first term in this equation represents the temporal evolution of the energy distribution, and the second term represents the propagation of particles along the jet, where $\Gamma(t,z)$ is the Lorentz factor along the jet and $v(t,z)$ its bulk velocity. Calculations including contributions from such terms of the transfer equation are going to be published in future works.

2.4. Gamma-Ray Source Function

In this subsection, we see the form of the source function of gamma-rays. For the source function of the other particles in the chains of reactions, one can see [31,32]. We have assumed that gamma-rays are mainly produced by π^0 decay. Besides this decay, gamma-rays can also be produced by the η meson decay as

$$\eta \longrightarrow \gamma+\gamma \quad (18)$$

The gamma-ray spectra are calculated for photons of energy $E_\gamma = xE_p$ through the expression (see Ref. [33])

$$F_\gamma(x,E_p)=B_\gamma\frac{lnx}{x}\left(\frac{1-x^{\beta_\gamma}}{1+k_\gamma x^{\beta_\gamma}(1-x^{\beta_\gamma})}\right)^4\left(\frac{1}{lnx}-\frac{4\beta_\gamma x^{\beta_\gamma}}{1-x^{\beta_\gamma}}-\frac{4k_\gamma\beta_\gamma x^{\beta_\gamma}(1-2x^{\beta_\gamma})}{1+k_\gamma x^{\beta_\gamma}(1-x^{\beta_\gamma})}\right) \quad (19)$$

where $B_\gamma = 1.3+0.14L+0.011L^2$, $\beta_\gamma = 1/(0.008L^2+0.11L+1.79)$, and $k_\gamma = 1/(0.014L^2+0.049L+0.801)$, where $L=\ln(E_p/1\text{ TeV})$. These results are consistent with proton energies in the range 0.1 TeV$< E_p < 10^5$ TeV. Equation (19) includes the contribution of η decay.

In the energy range $E_\gamma \geq 100$ GeV, the gamma-ray source function is

$$Q_\gamma(E_\gamma,z)=cn(z)\int_{E_\gamma/E_p^{max}}^1\frac{dx}{x}N_p\left(\frac{E_\gamma}{x},z\right)F_\gamma\left(x,\frac{E_\gamma}{x}\right)\sigma_{pp}^{(inel)}\left(\frac{E_\gamma}{x}\right) \quad (20)$$

The inelastic cross-section for the $p-p$ scattering is given by (see Refs. [33–35])

$$\sigma_{pp}^{(inel)}(E_p)=(0.25l^2+1.88L+34.3)\left(1-\left(\frac{E_{th}}{E_p}\right)^4\right)^2\times 10^{-27}\text{cm}^2 \quad (21)$$

where $L=\ln(E_p/1000)$, with E_p in GeV and $E_{th}=1.2$ GeV being the threshold energy for the production of a single neutral pion. For $E_\gamma < 100$ GeV, the delta-function approximation is used.

2.5. Intensities and Integral Fluxes

If we integrate the source function of Equation (20) over the acceleration zone, we obtain the respective intensity (see Refs. [36,37]) as

$$I_{\gamma,o}(E_\gamma)=\int_V Q_\gamma(E_\gamma,z)d^3r=\pi\tan^2\xi\int_{z_0}^{z_{max}}Q_\gamma(E_\gamma,z)z^2dz \quad (22)$$

where the second equality holds because of the conical geometry of the jet.

However, part of the photons emitted from the jet can be absorbed due to e^+-e^- production through the interaction:

$$\gamma+\gamma\longrightarrow e^++e^- \quad (23)$$

This can take place if a photon emitted from the jet interacts with a lower-energy photon emitted from the accretion disk, the donor (companion) star, or the corona. This leads to the

corresponding optical depths τ_{disk}, τ_{donor}, and τ_{cor}, which depend on various parameters of the binary system.

So, their initial intensity $I_{\gamma,0}$ will be reduced to

$$I_\gamma = I_{\gamma,o} e^{-\tau_{all}} \tag{24}$$

where τ_{all} is the sum of all the optical depths.

The corresponding photon integral flux emitted is calculated through

$$\Phi_\gamma = \int_{100}^{E_{max}} \frac{I_\gamma(E_\gamma) dE_\gamma}{4\pi d^2} \tag{25}$$

2.6. Absorption from the Accretion Disk

In this subsection, we discuss the photon absorption due to the interaction described by Equation (23). The accretion disk consists of overheated matter and gas rotating around the system's black hole. The mass accretion rate $\dot{M}_{accr}$ is defined as the rate at which mass from the donor star accumulates in the equatorial region of the black hole in a binary system. For the accretion disk of the system, we use the Shakura–Sunyaev "standard" disk model (see Ref. [38]), the best known and studied theoretical model. In this model, the accretion disk's inner radius is located at $R_{in} = R_{ISCO}$.

Due to the presence of the magnetic field and high temperature, the disk emits soft X-ray photons capable of absorbing the gamma-ray photons when they collide with an angle θ_0. The cross-section of this interaction is (see Ref. [39])

$$\sigma_{\gamma\gamma}(E_\gamma, \epsilon, \theta_0) = \frac{\pi e^4}{2m_e^2 c^4}(1-\beta^2)\left[(3-\beta^4)\ln\left(\frac{1+\beta}{1-\beta}\right) - 2\beta(2-\beta^2)\right] \tag{26}$$

where ϵ is the energy of the less energetic photon originating from the accretion disk. Also,

$$\beta = \sqrt{1-\frac{1}{s}}, \qquad s = \frac{\epsilon E_\gamma(1-\cos\theta_0)}{2m_e^2 c^4}$$

For pair creation to occur, $s > 1$.

The disk optical depth τ_{disk} is given by integrating over the X-ray photon energy, the distance that the high-energy photons travels from the emission source to the observer l, and the disk's radius R and angle ϕ:

$$\tau_{disk} = \int_0^\infty \int_0^{2\pi} \int_{R_{in}}^{R_{out}} \int_{\epsilon_{min}}^\infty \frac{dn}{d\epsilon d\Omega}(1-\cos\theta_0)\sigma_{\gamma\gamma}\frac{\rho\cos\omega}{D^3} R d\epsilon dR d\phi dl \tag{27}$$

where $\epsilon_{min} = 2m_e^2c^4/E_\gamma(1-\cos\theta_0)$, ρ is the collision point distance to the central object, D is the distance between the disk's surface element and the collision point, and ω is the angle between ρ and the z axis.

Analytically, the above quantities are

$$\rho = \left(z^2 + l^2 + 2lz\cos i\right)^{1/2}, \qquad D = \left(R^2 + \rho^2 - 2R\rho\cos\psi\right)^{1/2}$$
$$\psi = \cos^{-1}\left(\frac{l\sin i\cos\phi}{\rho}\right), \qquad \omega = \cos^{-1}\left(\frac{z + l\cos i}{\rho}\right)$$

where ψ is the angle between ρ and R, and i is the inclination angle of the jet's axis to the observer's line of sight. If we assume thermal equilibrium between the infinitesimal surface elements of the disk, the emitted photon density follows the black-body radiation spectrum:

$$\frac{dn}{d\epsilon d\Omega} = \frac{2}{h^2c^3}\frac{\epsilon^2}{e^{\mathcal{T}(R)} - 1} \tag{28}$$

where $\mathcal{T}(R) = \epsilon/k_B T(R)$ with k_B being the Boltzmann constant and h the Planck constant. As we have already mentioned, the disc begins at $R_{in} = R_{ISCO}$, with R_{ISCO} given by Equation (9).

For the temperature of the disk $T(R)$, we use the temperature profile which is obtained by the Paczyński–Wiita potential (see Ref. [40]):

$$\Phi_{PW} = -\frac{GM_{bh}}{r - r_S} \tag{29}$$

The latter equation gives the temperature profile (see Ref. [41]):

$$T(r) = T_o \left[\frac{\bar{r} - 2/3}{\bar{r}(\bar{r}-2)^3} \left(1 - \frac{3^{3/2}(\bar{r}-2)}{2^{1/2}\bar{r}^{3/2}} \right) \right]^{1/4} \tag{30}$$

where $\bar{r} = r/r_g$. Furthermore, the dependence on the black hole's mass and the accretion rate is sustained through the following constant:

$$T_o = \left(\frac{3GM_{BH}\dot{M}}{8\pi\sigma_{SB}r_g^3} \right)^{1/4}.$$

For a more realistic description of the accretion disk around a rotating black hole, we could incorporate the potential proposed from Mukhopadhyay [42]. From this potential, we can extract a temperature profile for the accretion disk [43] as

$$T(r) = T_o \left(\frac{4\mathcal{R}(\bar{r})^2}{3\bar{r}^4} - \mathcal{L}(\bar{r}) \right)^{1/4} \left(1 - \frac{\mathcal{R}(\bar{r}_{in})}{\mathcal{R}(\bar{r})} \right)^{1/4}, \tag{31}$$

where we have defined the following functions:

$$\mathcal{R}(\bar{r}) = \frac{\bar{r}^2 - 2\alpha_*\sqrt{\bar{r}} + \alpha_*^2}{\sqrt{\bar{r}}(\bar{r}-2) + \alpha_*}$$

$$\mathcal{L}(\bar{r}) = \frac{2\mathcal{R}(\bar{r})}{3\bar{r}^3\left(\sqrt{\bar{r}}(\bar{r}-2) + \alpha_*\right)} \left(2\bar{r} - \frac{\alpha_*}{\sqrt{\bar{r}}} - \frac{3\bar{r}-2}{2\sqrt{\bar{r}}}\mathcal{R}(\bar{r}) \right).$$

In future works, we will use the above temperature profile in our calculations [44].

3. Results and Discussion

The results obtained in this work refer to an ideal BHXRB system with parameters commonly found in typical BHXRBs. We set different values for the spin parameter of the black hole of the system in order to determine what effect it has on the results while changing it. The main parameters of the system are found in Table 1.

For the above parameters, we calculate the luminosity of the disk (L_{disk}) as a function of the photon energy of the disk's black-body spectrum, which is depicted in Figure 1 for various values of the dimensionless spin parameter α_*. As can be seen, the luminosity becomes significant for larger energy values as α_* increases. This occurs because as α_* increases, the R_{ISCO} becomes smaller, so the disk's inner radius (R_{in}) is located at a smaller radius where its temperature is higher. As a result of this, the black-body spectrum of the accretion disk increases.

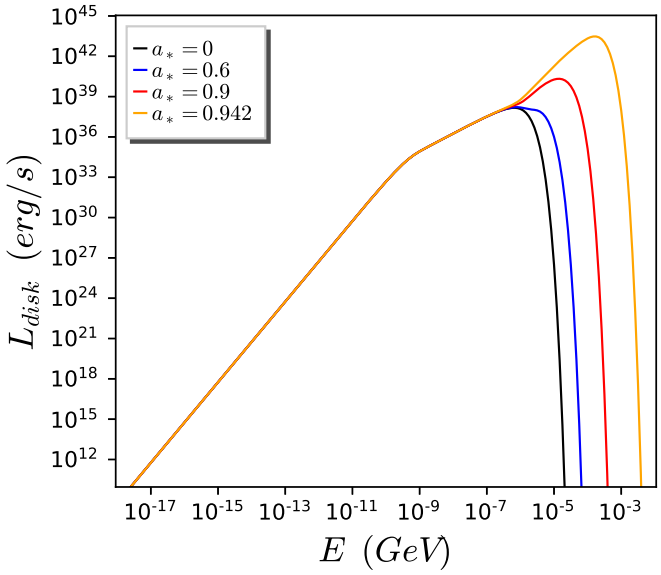

Figure 1. The luminosity (L_{disk}) of the disk with respect to photon energy (E) for various values of α_*.

Table 1. Main parameters of the ideal BHXRB system.

BHXRB Parameter	Symbol (Units)	Value
Black hole mass	$M_{bh}(\mathrm{M}_\odot)$	20
Donor star mass	$M_d(\mathrm{M}_\odot)$	15
Distance to Earth	d(kpc)	2
Donor star luminosity	$L_{star}(\mathrm{L}_\odot)$	10^4
Donor star temperature	T_d(K)	10,000
Jet's inclination	$i(^\circ)$	30
Jet's Lorentz factor	Γ_b(c)	2.29
Jet's half-opening angle	$\xi(^\circ)$	2.0
Black hole's spin parameter	α_*	$\pm 0, 0.6, 0.9$
Mass accretion rate	$\dot{M}(\dot{\mathrm{M}}_{\mathrm{Edd}})$	0.07
Jet's emitting region height	z_0(cm)	10^8
Seperation distance of the system	s(cm)	3.16×10^{12}

We also consider that the jet's hadron-to-lepton ratio is $\alpha_k = L_p/L_e = 1$, where L_p (L_e) stands for the proton (electron) kinetic luminosity. At this point we assume that a small portion of the particles, $q_r = 10^{-4}$, is accelerated in the acceleration zone of the jet.

In general, in BHXRB systems the acceleration zone of the jet is taken to be from $z_0 = 10^8$ cm (where z_0 represents the distance from the center of the black hole to the start of the acceleration zone) up to $z_{max} = 5 * z_0$ (where z_{max} denotes the distance from the center of the black hole to the end of the acceleration zone). The acceleration efficiency is taken to be $\eta = 0.1$.

For these parameters, we now calculate the exponential of minus all the optical depths that are found in Equation (24), which is shown in Figure 2. What we can see is that the larger the spin parameter, the larger the absorption, and when we go to negative values of α_*, the absorption is even smaller.

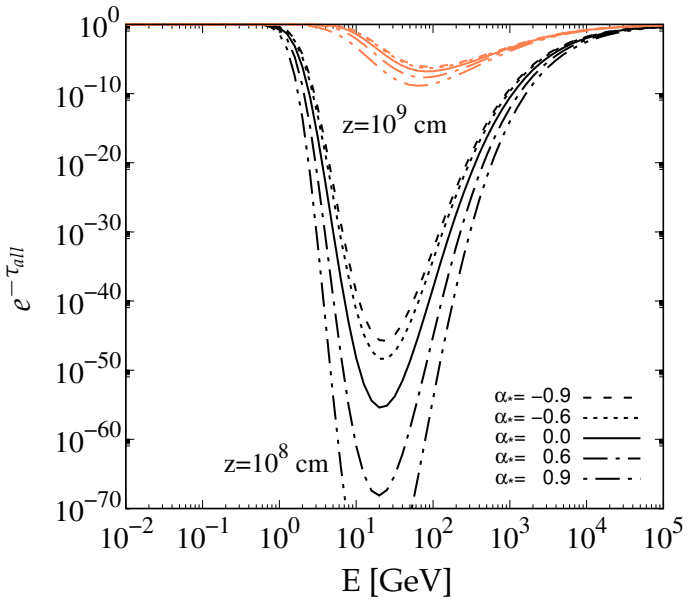

Figure 2. The exponential of minus the sum of the optical depths ($e^{-\tau_{all}}$) with respect to photon energy (E) for various values of α_*.

Considering a leptonic model, the radiation emission is produced by synchrotron emission from accelerated jet electrons and protons, and inverse Compton scattering [45] between disk photons and jet electrons. We have calculated the differential flux after absorption. It is depicted in Figure 3. We observe that the larger the spin, the lower the differential flux, while for negative values of α_*, the differential flux is larger.

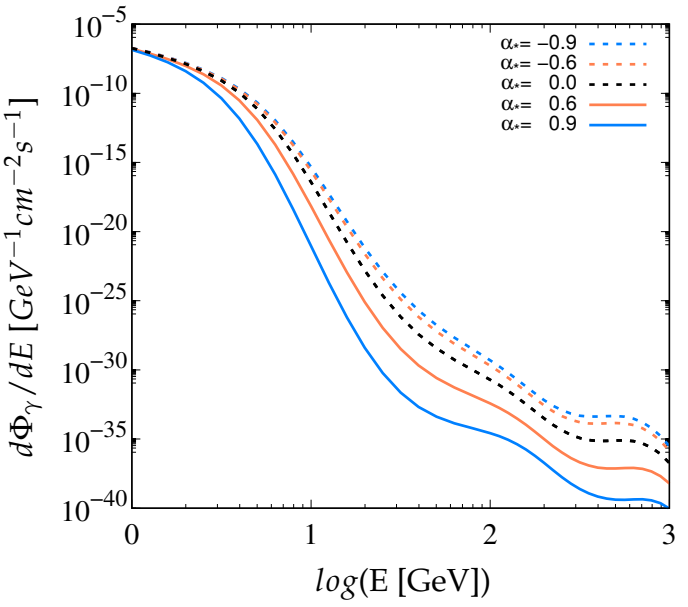

Figure 3. The differential flux ($d\Phi_\gamma/dE$) of synchrotron emission from accelerated jet electrons and protons and inverse Compton scattering between disk photons and jet electrons with respect to log E for various values of α_*.

We can conclude that for larger values of the spin parameter, we have more absorption and thus a lower differential flux. This can be explained by the value of the R_{ISCO}. For more negative values of the spin parameter, the R_{ISCO} is larger, so the accretion disk is smaller, and in this way, it absorbs less photons from the jet. On the other hand, going to larger

positive values of the spin parameter, the R_{ISCO} becomes smaller, so the accretion disk is larger and has higher temperatures, and in this way, it contributes more to the absorption.

In order to determine a more concrete conclusion from our results, our model should be applied to real observed BHXRB systems. Such systems could be the MAXI J1820+070 (see Refs. [46–54]), the XTE J1550-564 (see Refs. [55–59]), and the XTE J1859+226 (see Refs. [60–63]). These three systems have different values of a_*, while their other parameters are close, so by performing calculations for them, we can further determine the effect of the black hole's spin on the emitted spectra.

4. Conclusions

In this work we first addressed the R_{ISCO} in the Kerr geometry which depends on the dimensionless spin parameter a_*. We presented the main interactions that take place inside the jets leading to the production of gamma-rays, and the transfer equation that describes the particles' energy distribution. Also, we discussed the gamma-ray source function, from which the gamma-ray intensity as well as integral flux emanate. Further, we examined how photons emitted from the jet can be absorbed due to $e^+ - e^-$ pair creation.

Moreover, we obtained results for an ideal BHXRB system. Specifically we studied the accretion disk's luminosity, the absorption, and the differential flux remaining after the absorption effect. Having performed calculations for various values of the spin parameter a_*, we concluded the following. When the spin has more negative values, the absorption effect becomes weaker and, thus, the differential flux is larger. When the spin parameter increases (becomes more positive), a larger luminosity of the accretion disk occurs; therefore, the absorption effect is more intense and, thus, the differential flux becomes smaller.

Our next goal is to apply our model to real observed BHXRB systems, such as the MAXI J1820+070, the XTE J1550-564, and the XTE J1859+226, in order to obtain results for their neutrino and gamma-ray intensities and integral fluxes expected to be observed at Earth (see Ref. [44]).

Author Contributions: Conceptualization, T.K. and O.K.; methodology, O.K.; software, O.K.; validation, T.K. and O.K.; formal analysis, D.R. and T.P.; investigation, D.R. and T.P.; resources, T.K.; data curation, T.K. and O.K.; writing—original draft preparation, D.R.; writing—review and editing, D.R. and T.K.; visualization, T.P.; supervision, T.K. and O.K.; project administration, T.K. and O.K.; funding acquisition, T.K. All authors have read and agreed to the published version of the manuscript.

Funding: The authors Th.P., O.T.K., and T.S.K. wish to acknowledge financial support from the Association for Advancement of Research on Open Problems (OPRA Association, Tel Aviv, Israel) in Nuclear Physics & Particle Physics, project No 83241/ELKE-UoI.

Data Availability Statement: The datasets generated during and/or analyzed in the present study are available upon request from the corresponding author.

Conflicts of Interest: Author Odysseas Kosmas was employed by the company Conigital Ltd. The remaining authors declare that the research was conducted in the absence of any commercial or financial relationships that could be construed as a potential conflict of interest.

Abbreviations

The following abbreviations are used in this manuscript:

BHXRB	Black Hole X-ray Binary
R_{ISCO}	Radius of the Innermost Stable Circular Orbit

References

1. Schee, J.; Stuchlík, Z. Profiles of emission lines generated by rings orbiting braneworld Kerr black holes. *Gen. Relativ. Gravit.* **2009**, *41*, 1795–1818. [CrossRef]
2. Bambi, C. Testing the space-time geometry around black hole candidates with the analysis of the broad K α iron line. *Phys. Rev.* **2013**, *87* , 023007.
3. Bambi, C. Broad K α iron line from accretion disks around traversable wormholes. *Phys. Rev.* **2013**, *87*, 084039.

4. Johannsen, T.; Psaltis, D. Testing the no-hair theorem with observations in the electromagnetic spectrum. IV. Relativistically broadened iron lines. *Astrophys. J.* **2013**, *773*, 57. [CrossRef]
5. Jiang, J.; Bambi, C.; Steiner, J.F. Testing the Kerr nature of black hole candidates using iron line spectra in the CPR framework. *Astrophys. J.* **2015**, *811*, 130. [CrossRef]
6. Ni, Y.; Zhou, M.; Cardenas-Avendano, A.; Bambi, C.; Herdeiro, C.A.; Radu, E. Iron Kα line of Kerr black holes with scalar hair. *J. Cosmol. Astropart. Phys.* **2016**, *2016*, 049. [CrossRef]
7. Zhou, M.; Cardenas-Avendano, A.; Bambi, C.; Kleihaus, B.; Kunz, J. Search for astrophysical rotating Ellis wormholes with X-ray reflection spectroscopy. *Phys. Rev. D* **2016**, *94*, 024036. [CrossRef]
8. Bambi, C.; Abdikamalov, A.B.; Ayzenberg, D.; Cao, Z.; Liu, H.; Nampalliwar, S.; Tripathi, A.; Wang-Ji, J.; Xu, Y. relxill_nk: A Relativistic Reflection Model for Testing Einstein's Gravity. *Universe* **2018**, *4*, 79. [CrossRef]
9. Zhang, Y.; Abdikamalov, A.B.; Ayzenberg, D.; Bambi, C.; Dauser, T.; García, J.A.; Nampalliwar, S. About the Kerr Nature of the Stellar-mass Black Hole in GRS 1915+105. *Astrophys. J.* **2019**, *875*, 41.
10. Kerr, R.P. Gravitational field of a spinning mass as an example of algebraically special metrics. *Phys. Rev. Lett.* **1963**, *11*, 237. [CrossRef]
11. Romero, G.E.; Vila, G.S. *Introduction to Black Hole Astrophysics*; Springer: Berlin/Heidelberg, Germany, 2013; Volume 876.
12. Newman, E.T.; Couch, E.; Chinnapared, K.; Exton, A.; Prakash, A.; Torrence, R. Metric of a rotating, charged mass. *J. Math. Phys.* **1965**, *6*, 918–919. [CrossRef]
13. McClintock, J.E.; Narayan, R.; Davis, S.W.; Gou, L.; Kulkarni, A.; Orosz, J.A.; Penna, R.F.; Remillard, R.A.; Steiner, J.F. Measuring the spins of accreting black holes. *Class. Quantum Gravity* **2011**, *28*, 114009. [CrossRef]
14. Papavasileiou, T.V.; Kosmas, O.T.; Sinatkas, I. Prediction of gamma-ray emission from Cygnus X-1, SS 433, and GRS 1915+105 after absorption. *Astron. Astrophys.* **2023**, *673*, A162. [CrossRef]
15. Papavasileiou, T.V.; Kosmas, O.T.; Sinatkas, I. Studying the Spectral Energy Distributions Emanating from Regular Galactic XRBs. *Universe* **2023**, *9*, 312. [CrossRef]
16. Kosmas, O.T.; Papavasileiou, T.V.; Kosmas, T.S. Integral Fluxes of Neutrinos and Gamma-Rays Emitted from Neighboring X-ray Binaries. *Universe* **2023**, *9*, 517. [CrossRef]
17. Hobson, M.P.; Efstathiou, G.P.; Lasenby, A.N. *General Relativity: An Introduction for Physicists*; Cambridge University Press: New York, NY, USA, 2006; pp. 310–354.
18. Bardeen, J.M.; Press, W.H.; Teukolsky, S.A. Rotating black holes: Locally nonrotating frames, energy extraction, and scalar synchrotron radiation. *Astrophys. J.* **1972**, *178*, 347–370. [CrossRef]
19. Böttcher, M.; Dermer, C.D. Photon-Photon Absorption of Very High Energy Gamma Rays from Microquasars: Application to LS 5039. *Astrophys. J.* **2005**, *634*, L81–L84. [CrossRef]
20. Cerutti, B.; Dubus, G.; Malzac, J.; Szostek, A.; Belmont, R.; Zdziarski, A.A.; Henri, G. Absorption of high-energy gamma rays in Cygnus X-3. *Astron. Astrophys.* **2011**, *529*, A120. [CrossRef]
21. Romero, G.E.; Vila, G.S. The proton low-mass microquasar: High-energy emission. *Astron. Astrophys.* **2008**, *485*, 623–631. [CrossRef]
22. Mannheim, K.; Schlickeiser, R. Interactions of cosmic ray nuclei. *Astron. Astrophys.* **1994**, *286*, 983–996.
23. Smponias, T.; Kosmas, O.T. Neutrino Emission from Magnetized Microquasar Jets. *Adv. High Energy Phys.* **2017**, *2017*, 4962741. [CrossRef]
24. Romero, G.E.; Torres, D.F.; Kaufman Bernadó, M.M.; Mirabel, I.F. Hadronic gamma-ray emission from windy microquasars. *Astron. Astrophys.* **2003**, *410*, L1–L4. [CrossRef]
25. Zhang, J.F.; Li, Z.R.; Xiang, F.Y.; Lu, J.F. Electron transport with re-acceleration and radiation in the jets of X-ray binaries. *Mon. Not. R. Astron. Soc.* **2017**, *473*, 3211–3222. [CrossRef]
26. Kosmas, O.T.; Leyendecker, S. Phase lag analysis of variational integrators using interpolation techniques. *PAMM Proc. Appl. Math. Mech.* **2012**, *12*, 677–678.
27. Kosmas, O.T.; Leyendecker, S. Family of high order exponential variational integrators for split potential systems. *J. Phys. Conf. Ser.* **2015**, *574*, 012002. [CrossRef]
28. Kosmas, O.T.; Vlachos, D.S. A space-time geodesic approach for phase fitted variational integrators. *Phys. Conf. Ser.* **2016**, *738*, 012133. [CrossRef]
29. Kantzas, D.; Markoff, S.; Beuchert, T.; Lucchini, M.; Chhotray, A.; Ceccobello, C.; Tetarenko, A.J.; Miller-Jones, J.C.A.; Bremer, M.; Garcia, J.A.; et al. A new lepto-hadronic model applied to the first simultaneous multiwavelength data set for Cygnus X–1. *Mon. Not. R. Astron. Soc.* **2021**, *500*, 2112–2126. [CrossRef]
30. Carulli, A.M.; Reynoso, M.M.; Romero, G.E. Neutrino production in Population III microquasars. *Astropart. Phys.* **2021**, *128*, 102557. [CrossRef]
31. Papavasileiou, T.; Kosmas, O.; Sinatkas, I. Simulations of Neutrino and Gamma-Ray Production from Relativistic Black-Hole Microquasar Jets. *Galaxies* **2021**, *9*, 67. [CrossRef]
32. Papavasileiou, T.; Kosmas, O.; Sinatkas, I. Relativistic Magnetized Astrophysical Plasma Outflows in Black-Hole Microquasars. *Symmetry* **2022**, *14*, 485. [CrossRef]
33. Kelner, S.R.; Aharonian, F.A.; Bugayov, V.V. Energy spectra of gamma rays, electrons, and neutrinos produced at proton-proton interactions in the very high energy regime. *Phys. Rev. D* **2006**, *74*, 034018. [CrossRef]

34. Smponias, T.; Kosmas, O.T. High Energy Neutrino Emission from Astrophysical Jets in the Galaxy. *Adv. High Energy Phys.* **2015**, *2015*, 921757. [CrossRef]
35. Kosmas, O.; Smponias, T. Simulations of Gamma-Ray Emission from Magnetized Microquasar Jets. *J. Adv. High Energy Phys.* **2018**, *2018*, 9602960. [CrossRef]
36. Reynoso, M.M.; Romero, G.E.; Christiansen, H.R. Production of gamma rays and neutrinos in the dark jets of the microquasar SS433. *Mon. Not. R. Astron. Soc.* **2008**, *387*, 1745–1754. [CrossRef]
37. Reynoso, M.M.; Romero, G.E. Magnetic field effects on neutrino production in microquasars. *Astron. Astrophys.* **2009**, *493*, 1–111. [CrossRef]
38. Shakura, N.I.; Sunyaev, R.S. Black holes in binary systems. Observational appearance. *Astron. Astrophys.* **1973**, *24*, 337–355.
39. Gould, R.J.; Schréder, G.P. Pair production in photon-photon collisions. *Phys. Rev.* **1967**, *155*, 1404. [CrossRef]
40. Paczynsky, B.; Wiita, P.J. Thick accretion disks and supercritical luminosities. *Astron. Astrophys.* **1980**, *88*, 23–31.
41. Gierliński, M.; Zdziarski, A.A.; Poutanen, J.; Coppi, P.S.; Ebisawa, K.; Johnson, W.N. Radiation mechanisms and geometry of Cygnus X-1 in the soft state. *Mon. Not. R. Astron. Soc.* **1999**, *309*, 492–512. [CrossRef]
42. Mukhopadhyay, B. Description of pseudo-Newtonian potential for the relativistic accretion disks around Kerr black holes. *Astrophys. J.* **2002**, *581*, 427. [CrossRef]
43. Papavasileiou, T.V.; Kosmas, O.; Kosmas, T.S. A direct method for reproducing fully relativistic spectra from standard accretion disks by modifying their inner boundary. *arXiv* **2024**, arXiv:2408.02415.
44. Rarras, D.; Kosmas, O.; Papavasileiou, T.; Kosmas, T. Black Hole's Spin-Dependence of γ-ray and Neutrino Emissions from MAXI J1820+070, XTE J1550-564, and XTE J1859+226. *Particles* **2024**. *to be published*.
45. Blumenthal, G.R.; Gould, R.J. Bremsstrahlung, synchrotron radiation, and compton scattering of high-energy electrons traversing dilute gases. *Rev. Mod. Phys.* **1970**, *42*, 237. [CrossRef]
46. Torres, M.A.P.; Casares, J.; Jiménez-Ibarra, F.; Álvarez-Hernández, A.; Muñoz-Darias, T.; Padilla, M.A.; Jonker, P.G.; Heida, M. The binary mass ratio in the black hole transient MAXI J1820+070. *Astrophys. J. Lett.* **2020**, *893*, L37. [CrossRef]
47. Mikołajewska, J.; Zdziarski, A.A.; Ziółkowski, J.; Torres, M.A.; Casares, J. The Donor of the Black Hole X-ray Binary MAXI J1820+070. *Astrophys. J.* **2022**, *930*, 9. [CrossRef]
48. Poutanen, J.; Veledina, A.; Berdyugin, A.V.; Berdyugina, S.V.; Jermak, H.; Jonker, P.G.; Kajava, J.J.E.; Kosenkov, I.A.; Kravtsov, V.; Piirola, V.; et al. Black hole spin–orbit misalignment in the X-ray binary MAXI J1820+070. *Science* **2022**, *375*, 874–876. [CrossRef]
49. Kalogera, V. Spin-orbit misalignment in close binaries with two compact objects. *Astrophys. J.* **2000**, *541*, 319. [CrossRef]
50. Atri, P.; Miller-Jones, J.C.A.; Bahramian, A.; Plotkin, R.M.; Deller, A.T.; Jonker, P.G.; Maccarone, T.J.; Sivakoff, G.R.; Soria, R.; Altamirano, D.; et al. A radio parallax to the black hole X-ray binary MAXI J1820+070. *Mon. Not. R. Astron. Soc. Lett.* **2020**, *493*, L81–L86. [CrossRef]
51. Zdziarski, A.A.; Tetarenko, A.J.; Sikora, M. Jet Parameters in the Black Hole X-ray Binary MAXI J1820+070. *Astrophys. J.* **2022**, *925*, 189. [CrossRef]
52. Zhao, X.; Gou, L.; Dong, Y.; Tuo, Y.; Liao, Z.; Li, Y.; Jia, N.; Feng, Y.; Steiner, J.F. Estimating the black hole spin for the X-ray binary MAXI J1820+070. *Astrophys. J.* **2021**, *916*, 108. [CrossRef]
53. Draghis, P.A.; Miller, J.M.; Zoghbi, A.; Reynolds, M.; Costantini, E.; Gallo, L.C.; Tomsick, J.A. A systematic view of ten new black hole spins. *Astrophys. J.* **2023**, *945*, 19. [CrossRef]
54. Bhargava, Y.; Belloni, T.; Bhattacharya, D.; Motta, S.; Ponti, G. A timing-based estimate of the spin of the black hole in MAXI J1820+070. *Mon. Not. R. Astron. Soc.* **2021**, *508*, 3104–3110. [CrossRef]
55. Orosz, J.A.; Steiner, J.F.; McClintock, J.E.; Torres, M.A.; Remillard, R.A.; Bailyn, C.D.; Miller, J.M. An improved dynamical model for the microquasar XTE J1550-564. *Astrophys. J.* **2011**, *730*, 75. [CrossRef]
56. Miller-Jones, J.C.A.; Fender, R.P.; Nakar, E. Opening angles, Lorentz factors and confinement of X-ray binary jets. *Mon. Not. R. Astron. Soc.* **2006**, *367*, 1432–1440. [CrossRef]
57. Motta, S.E.; Munoz-Darias, T.; Sanna, A.; Fender, R.; Belloni, T.; Stella, L. Black hole spin measurements through the relativistic precession model: XTE J1550-564. *Mon. Not. R. Astron. Soc. Lett.* **2014**, *439*, L56–L69. [CrossRef]
58. Steiner, J.F.; Reis, R.C.; McClintock, J.E.; Narayan, R.; Remillard, R.A.; Orosz, J.A.; Gou, L.; Fabian, A.C.; Torres, M.A.P. The spin of the black hole microquasar XTE J1550-564 via the continuum-fitting and Fe-line methods. *Mon. Not. R. Astron. Soc.* **2011**, *416*, 941–958. [CrossRef]
59. Kaaret, P.; Corbel, S.; Tomsick, J.A.; Fender, R.; Miller, J.M.; Orosz, J.A. Tzioumis, A.K.; Wijnands, R. X-ray Emission from the Jets of XTE J1550-564. *Astrophys. J.* **2003**, *582*, 945. [CrossRef]
60. Nandi, A.; Mandal, S.; Sreehari, H.; Radhika, D.; Das, S.; Chattopadhyay, I.; Iyer, N.; Agrawal, V.K.; Aktar, R. Accretion flow dynamics during 1999 outburst of XTE J1859+ 226-modeling of broadband spectra and constraining the source mass. *Astrophys. Space Sci.* **2018**, *363*, 1–12. [CrossRef]
61. Kimura, M.; Done, C. Evolution of X-ray irradiation during the 1999–2000 outburst of the black hole binary XTE J1859+ 226. *Mon. Not. R. Astron. Soc.* **2019**, *482*, 626–638. [CrossRef]

62. Yanes-Rizo, I.V.; Torres, M.A.P.; Casares, J.; Motta, S.E.; Muñoz-Darias, T.; Rodríguez-Gil, P.; Armas Padilla, M.; Jiménez-Ibarra, F.; Jonker, P.G.; Corral-Santana, J.M.; et al. A refined dynamical mass for the black hole in the X-ray transient XTE J1859+ 226. *Mon. Not. R. Astron. Soc.* **2022**, *517*, 1476–1482. [CrossRef]
63. Motta, S.E.; Belloni, T.; Stella, L.; Pappas, G.; Casares, J.; Muñoz-Darias, A.T.; Torres, M.A.P.; Yanes-Rizo, I.V. Black hole mass and spin measurements through the relativistic precession model: XTE J1859+ 226. *Mon. Not. R. Astron. Soc.* **2022**, *517*, 1469–1475. [CrossRef]